A spheroidal weathering model coupling porewater chemistry to soil thicknesses during steady state denudation

R. C. Fletcher, H. L. Buss, S. L. Brantley, Earth and Environmental Systems Institute, The Pennsylvania State University, University Park, PA 16802*

Abstract

Spheroidal weathering, a common mechanism that initiates the transformation of bedrock to saprolite, creates concentric fractures demarcating relatively unaltered corestones and progressively more altered rindlets. In the spheroidally weathering Rio Blanco quartz diorite (Puerto Rico), diffusion of oxygen into corestones initiates oxidation of ferrous minerals and precipitation of ferric oxides. A positive ΔV of reaction results in the build-up of elastic strain energy in the rock. Formation of each fracture is postulated to occur when the strain energy in a layer equals the fracture surface energy. The rate of spheroidal weathering is thus a function of the concentration of reactants, the reaction rate, the rate of transport, and the mechanical properties of the rock. Substitution of reasonable values for the parameters involved in the model produces results consistent with the observed thickness of rindlets in the Rio Icacos bedrock (≈ 2-3 cm) and a time interval between fractures (≈ 200-300 a) based on an assumption of steady-state denudation at the measured rate of 0.01 cm/a. Averaged over times longer than this interval, the rate of advance of the bedrock-saprolite interface during spheroidal weathering (the weathering advance rate) is constant with time. Assuming that the oxygen concentration at the bedrock-saprolite interface varies with the thickness of soil/saprolite yields predictive equations for how weathering advance rate and steady-state saprolite/soil thickness depend upon atmospheric oxygen levels and upon denudation rate. The denudation and weathering advance rates at steady state are therefore related through a condition on the concentration of porewater oxygen at the base of the saprolite. In our model for spheroidal weathering of the Rio Blanco quartz diorite, fractures occur every ~ 250 years, ferric oxide is fully depleted over a four rindlet set in ~ 1000 years, and saprolitization is completed in ~ 5000 years in the zone

containing ~ 20 rindlets. Spheroidal weathering thus allows weathering to keep up with the high rate of denudation by enhancing access of bedrock to reactants by fracturing. Coupling of denudation and weathering advance rates can also occur for the case that weathering occurs without spheroidal fractures, but for the same kinetics and transport parameters, the maximum rate of saprolitization achieved would be far smaller than the rate of denudation for the Rio Blanco system. The spheroidal weathering model provides a quantitative picture of how physical and chemical processes can be coupled explicitly during bedrock alteration to soil to explain weathering advance rates that are constant in time.

* Corresponding author, email: rfletche@geosc.psu.edu, fax: (814) 865-3191
Keywords: Spheroidal weathering, saprolite, steady state, soil, erosion

Introduction

Regolith formation rates from bedrock are largely unknown, although rates on the order of 0.005 [1] to ~0.1 mm/y [2] have been estimated. Such rates are generally based upon the untested assumption of a steady-state soil thickness [3]. To maintain a steady state soil thickness on weathering bedrock, the rate of transformation of saprolite to soil must equal that of bedrock to saprolite. The latter rate, here termed the weathering advance rate, ω, must also equal the rate of total denudation, R, for a steady state system. While several researchers have documented evidence suggesting that chemical weathering rates may vary proportionally with total denudation rates, no model has been described that explains why the weathering advance rate and total denudation rate should be equal, as required to maintain steady state soil thickness [3]. Here we present such a model for the case of a common saprolite formation mechanism, spheroidal weathering.

Spheroidal weathering, also termed concentric or onion-skin weathering, is a process whereby concentric shells (Fig. 1a) of intact but weathered rock form sequentially by fracture of weakly altered bedrock [4]. Spheroidal weathering has been observed on almost all rock types including gneiss, schist, andesite, sandstone, and greywacke and in almost every climate; however, the phenomenon is most common in homogeneous, jointed, coherent rocks, primarily granites and basalts [5-8]. It is not

known why some rocks weather spheroidally, developing corestones, and others do not, although ease of grain disaggregation has been suggested as a contributor [9]. Granitic corestones have been identified in a variety of climatic regions on all continents except Antarctica. Some have proposed that the percentage of biotite [10] or feldspar [11] controls susceptibility to spheroidal weathering. Some have asserted the importance of climate[12, 13] while others have argued against climate as a primary control[14, 15].

Geologic setting and observations

The Rio Icacos watershed in the Luquillo Experimental Forest in Puerto Rico has one of the highest documented chemical weathering rates of granitic rocks in the world[16]. The weathering Tertiary-age Rio Blanco quartz diorite is capped with 2–8 m of saprolite overlain by another 0.5–1 m of soil[16-22]. The rate of advance of the weathering front has been estimated at approximately 1 cm per 100 years based upon cosmogenic evidence[23]. The transition between the coarse-grained Rio Blanco quartz diorite and the saprolite is not a sharp interface, but consists rather of a 20-60 cm-thick zone characterized by fracture-bound concentric shells, termed here rindlets [7] (Fig. 1), caused by spheroidal weathering; the zone itself is termed a rindlet sequence.

The 2-8 meter-thick saprolite overlying the intact quartz diorite is depleted in Na, Ca, and Mg compared to bedrock due to preferential weathering of the primary minerals plagioclase and hornblende[16, 22]. Plagioclase and hornblende are present at 40 and 15 volume percent respectively in the bedrock, but are dissolved completely between the bedrock and saprolite. Biotite, at 5 volume percent in bedrock, begins to weather in the bedrock but is present in saprolite, where it continues to weather [16, 18].

Rindlets were observed in cross-section in a road cut, and in plan section on a fresh landslide scour. In the latter, they are demarcated by vertically-stacked overlapping equant cracks with diameters of 1 to 4 m that represent penetration of weathering into un-jointed granite along a sub-planar front. In the former, rindlet sequences penetrate along steep joints to partially or completely surround joint-bounded corestones, but otherwise form a continuous sub-planar boundary zone between saprolite and bedrock. While the concentric shells of partly weathered rock surrounding fracture-bounded blocks of fresh rock comprise the visually-prominent form of spheroidal weathering from which the

name is derived, these examples serve to motivate the geometrically simpler one-dimensional model presented here. In this model, the shells or rindlets have zero curvature and unbounded lateral extent.

In both outcrops, individual rindlet thicknesses range from ~ 0.3 – 10 cm, with a mean value of 2.6 cm $\pm$ 1.6 cm (1σ). While a moderate decrease in rindlet thickness is sometimes observed at increasing distance from the corestone, this appears to be a second-order effect related to the further propagation of rindlet-bounding cracks. Profiles of rindlet thickness as a function of distance from the corestone are shown in Figure 2. In these examples, the total rindlet sequence measures ~ 40 cm in thickness and contains 14 - 20 rindlets.

In thin section, no significant porosity is visible in the corestone, whereas rindlets contain multiple irregular cracks or channels cutting through and around mineral grains without preference (Fig. 3). Mineral grains along channels are cut by multiple cracks and have more void space in and around them, indicating that the channels allow water penetration. Fe-oxide and clay mineral precipitates of sub-grain dimension are also observed near cracks.

Spheroidal weathering model

To develop a model that predicts the rate that bedrock transforms to saprolite, a mechanism driving spheroidal weathering must be delineated and quantified. A number of researchers have suggested that an increase in volume during mineral weathering could induce spheroidal cracking[6, 12, 24, 25]. Some have suggested that a larger modal per cent of biotite[10] or feldspar [11] favors such cracking. To our knowledge, no quantitative physical-chemical model has been proposed.

Based upon literature and petrographic observations, we identified three candidate families of reaction that are observed to be altering volumetrically significant minerals at the bedrock-saprolite interface in the Rio Blanco quartz diorite: plagioclase alteration to clay, hornblende alteration to Fe oxides, vermiculite and/or smectite[26, 27], and biotite alteration to hematite, vermiculite, or kaolinite[18, 28-31]. Of these three candidates, only reactions incorporating alteration of Fe minerals[32] have a positive ΔV of reaction, where V is the molar volume of solid phase products or reactants:

$$\Delta V = \sum V_{products} - \sum V_{reactants} \quad (1)$$

We model this type of reaction as the oxidative dissolution of the FeO component in the rock followed by precipitation of ferrihydrite, $Fe(OH)_{3\,(s)}$:

$$FeO_{(s)} + \frac{3}{2}H_2O + \frac{1}{4}O_2 \rightarrow Fe(OH)_{3(s)} \quad (2)$$

We assume that the rate of oxidative dissolution of the FeO component is slow, and thus rate-controlling, while the precipitation of ferrihydrite is effectively instantaneous and quantitative. The rate of consumption, Q, of O_2 (mol O_2 cm_{rock}^{-3} s^{-1}) is therefore controlled by the rate of reaction 2, which is dependent upon the activity of FeO in the rock, a_{FeO}:

$$Q = rk'S\rho f_o a_{FeO} c^{0.25} \quad (3)$$

Here, r is the stoichiometric coefficient in (2) describing the moles of dioxygen consumed per mole of reacting FeO (r = 0.25), k' is the kinetic constant for oxidative dissolution of the FeO component normalized by the surface area of FeO (mol Fe $M^{-0.25}$ m^{-2} s^{-1}), and c is the concentration of dissolved O_2 (M) in pore fluid. We have assumed that the rate of reaction of FeO is proportional to c^r and a_{FeO}. To obtain the desired units for Q, the product of specific surface area (S, m^2 gm^{-1}), density (ρ, gm cm^{-3}), and initial volume fraction (f_o) of the reacting ferrous component is included in (3). To express Q as a function of a dimensionless concentration $C = c/c_R$, where c_R is a reservoir concentration (see equation 9), we multiply the kinetic constant k' by $(c_R)^{0.25}$ to yield k (mol Fe m^{-2} s^{-1}) and replace $c^{0.25}$ by $C^{0.25}$: the kinetic constant k can be conceptualized as the rate constant for dissolution of the FeO component. This FeO component is largely hosted in biotite and hornblende in the Rio Blanco stock.

The activity of FeO in (3) can be estimated as the product of the initial mole fraction of FeO, M (moles FeO per mole of total oxides in the rock), multiplied by a term involving the extent of reaction, ξ, defined as the moles FeO reacted divided by the initial number of moles of FeO in the rock:

$$a_{FeO} = M(1-\xi) \quad (4)$$

With these two modifications to the expression for Q, we obtain:

$$Q = rkS\rho f_o M(1-\xi)C^{0.25} \tag{5}$$

Q is assumed nonzero for all values of c greater than the nucleation cut-off, c_N. Below this concentration of porefluid oxygen, the driving force for precipitation is assumed to be too small to nucleate ferrihydrite, and $Q = 0$.

Diffusive transport and reaction of O_2 satisfies the equation:

$$\phi\frac{\partial c}{\partial t} = \frac{D\phi^m}{\tau}\frac{\partial^2 c}{\partial x^2} - Q \tag{6}$$

where D is diffusivity in bulk fluid, ϕ is porosity, and m is the power of the porosity in the expression for the effective diffusivity and τ is tortuosity. The extent of reaction, ξ, can be written as a function of consumption rate of O_2 and the molar volume of FeO (V_{FeO}, $cm^3\ mol^{-1}$):

$$\frac{\partial \xi}{\partial t} = \left(\frac{V_{FeO}}{rf_o}\right)Q \tag{7}$$

In implementing the model, we use an initial condition of unreacted corestone in contact with an overlying porefluid reservoir. Defining x as the distance inward from this contact (x = 0) and t as the elapsed time, the initial conditions for solution of these equations are:

$$\begin{aligned} c(x,0) &= c_{eq} \cong 0 \\ \xi(x,0) &= 0 \end{aligned} \tag{8}$$

for all values of x > 0. The boundary condition at x = 0 is:

$$c(0,t) = c_R \tag{9}$$

where c_R is the concentration of O_2 in pore fluid at the saprolite-bedrock interface. Here, c_{eq} is the equilibrium concentration of O_2 within pore fluid in equilibrium with the unaltered rock.

As ferrihydrite precipitates, the ΔV of reaction results in accumulation of elastic strain energy. A fracture is postulated to form when the elastic strain energy per unit area of altering corestone produced during formation of ferrihydrite is equivalent to the

surface energy of fracture, 2Γ. This is a necessary condition for fracture, but does not embody any of the details of the fracture process. The time elapsed until the first crack forms is t_{crack}: as will be demonstrated below, the time interval between formation of subsequent cracks is nearly identical in magnitude. To calculate the elastic strain energy, we integrate the strain energy density, U, inward from the pristine bedrock surface or from the last-formed crack to the position where $c = c_N$:

$$\int_{x_j}^{x_{j+1}} U(x)dx = 2\Gamma \tag{10}$$

Here, x_j is the position of the initial saprolite-corestone contact, or the last fracture to form. The elastic strain energy density is:

$$U\left(x\right) = \frac{E\varepsilon^2}{\left(1-\nu\right)} \tag{11}$$

where E is Young's Modulus and ν is Poisson's Ratio. In computing this result, the mechanical constraint of zero strain (elastic and inelastic) parallel to the weathering front is taken into account. The linear inelastic strain from the bulk expansion is:

$$\varepsilon = \frac{\xi f_0}{3}\left(\frac{V_{Fe(OH)_3} - V_{FeO}}{V_{FeO}}\right) = \frac{\xi f_0}{3}\frac{\Delta V}{V} \tag{12}$$

Transport of reacting oxygen from an overlying reservoir into newly opened rindlet-bounding fractures is assumed sufficiently rapid that the concentration of dissolved O_2 is equal to the value, c_R, in each fracture immediately after fracture formation. When a rindlet separates from the corestone, many internal cracks form within it, as noted above, facilitating this rapid transport into the rindlet-bounding fractures.

For computational purposes, the above system of equations and conditions is cast into dimensionless form:

$$\begin{aligned} \frac{\partial C}{\partial T} &= \frac{\partial^2 C}{\partial X^2} - \Lambda C^{\frac{1}{4}}\left(1-\xi\right) \\ \frac{\partial \xi}{\partial T} &= \alpha C^{\frac{1}{4}}\left(1-\xi\right) \end{aligned} \tag{13}$$

Reaction only occurs for $C \geq C_N$. The dimensionless form of the fracture condition (10) is:

$$\int_{X_j}^{X_{j+1}} \xi^2 dX = 1 \tag{14}$$

The characteristic time and length are:

$$t^* = \frac{\tau \left(x^* \right)^2}{D\phi^{m-1}}$$
$$x^* = \frac{2\Gamma\left(1-\nu\right)}{E\left(\frac{f_0}{3} \frac{\Delta V}{V} \right)^2} \tag{15}$$

the dimensionless variables are:

$$C = \frac{c}{c_R}, C_N = \frac{c_N}{c_R}$$
$$X = \frac{x}{x^*} \tag{16}$$
$$T = \frac{t}{t^*}$$

and the dimensionless groups are:

$$\Lambda = \frac{rkSM\rho f_0 t^*}{\phi c_R} \tag{17}$$
$$\alpha = V_{FeO} kSM\rho f_o t*$$

The above system of equations is solved using a finite-difference method, with the fracture condition (14) tested at each time step.

Model results

The model yields profiles of the fraction of mineral reacted, ξ(X, T), and of concentration of the diffusing reactant, C(X, T). The initial condition, reservoir fluid in contact with unreacted corestone, is adopted here although it is somewhat artificial. In addition, the model only follows the FeO reaction and thus cannot address the final transformation of rindlets to saprolite. Transformation of rindlet to saprolite, dictated largely by alteration of plagioclase to clay, determines the width of the rindlet zone (40-

60 cm thick in the Rio Blanco). For comparison to the Rio Blanco system, we run the spheroidal weathering model to produce profiles of comparable width with ~15 rindlets.

To emphasize the significance of fracture formation within the full model formulation (Figure 4b), a model is also calculated with diffusion and reaction but no fracture (Figure 4a). Models with and without fracture are shown as four profiles of ξ and C for the same dimensionless times T = 4 x 10^8, 8 x 10^8, 12 x 10^8, and 16 x 10^8. Both cases are calculated using values of the dimensionless parameters Λ =0.0572 and α =6.32×10^{-9}, and for a dimensionless nucleation cut-off of C_N = 0.1. These values correspond to the model that fits the field observations.

For both cases, an initial transient state occurs wherein the extent of reaction in the outermost layer or rindlet is less than 100%; eventually the outer layer of the corestone (no-fracture case) or first formed rindlet (with-fracture case) has no reacting mineral remaining. For both cases this transient, T_{trans}, ≈ 8 x 10^8. Once T > T_{trans}, the profile of concentration of reacted mineral (the reaction front) is constant across the outermost layer of corestone (non-fracture case) or across the rindlet sets (fracture case), although the weathering interface is moving downward with time. Such a constant but moving reaction front is expected for some weathering systems, and is termed a quasi-stationary state [33]. For $\alpha << \Lambda$ as in our system, the product αT controls the form of this quasi-stationary reaction front and its position with time.

In the no-fracture case, the reaction front penetrates to a depth X ≈ 11 at T = 16 x 10^8, and the penetration depth of the zone of 100% reacted FeO varies approximately as $T^{0.4}$. If a very low value of C_N is used, the position of the reaction front is proportional to $\sqrt{T}$, a result expected for diffusional rate-control [33], as in so-called parabolic kinetics. In the fracture case, the reaction front reaches a depth X ≈ 80 at T = 16 x 10^8. In contrast to the no-fracture case, the rate of penetration of the reaction front is constant in T, reflecting the production of another rindlet by fracture after every time increment t_{crack} (= $T_{crack}t^*$).

The normalized widths of successive rindlets, W/x^*, and the normalized time intervals between fracture events, t_{crack}/t^*, were determined for a matrix of the dimensionless parameters α and Λ. Approximate expressions were derived to fit the

results for $C_N = 0.1$ in the parameter range of interest for $\Lambda >> \alpha$, the parameter range shown to fit model and field observations. These expressions are summarized in the following equations for the distance between fractures, *W*, and time between fractures:

$$W \cong 1.44 x^* \sqrt{\frac{1}{\Lambda}}$$
$$t_{crack} = 2.18 \left(\frac{\Lambda^{\frac{3}{10}}}{\alpha} \right) t^* \qquad (18)$$

The powers of Λ and α here are approximations to the fits from the numerical results – e.g., the best-fit exponent of Λ obtained for the expression for *W* is –0.47 rather than –0.5.

Application to observed weathering profiles

To establish a potential fit of the model to field observations, the following procedure was used. Many of the model parameters may be assigned values with small uncertainty relative to those that have much larger uncertainties. These are (see Table 1 for values): V_{FeO}, ρ, $\Delta V/V$, and r, based on reaction (2); f_0 and *M* from mineral and chemical analysis of the corestone; and c_R from a field measurement. The tortuosity is given a conventional value $\tau = 3$, and Poisson's ratio is set to a representative value, $\nu = 0.25$.

This leaves the seven parameters: E, Γ, k, S, D, ϕ, and m. If Γ ranges from 2 x 10^5 dyne/cm^2 to 5 x 10^5 dyne/cm^2 and E ranges from 10^{11} dyne/cm^2 to 10^{12} dyne/cm^2, $(\Gamma \times 10^6)/E$ has the modest range from 0.2 to 5. Here, the value of Γ is obtained for tensile fracture in polycrystalline rock [34]; values from single crystals are smaller by a factor of ~ 0.01 and values obtained for shear fractures are larger by a factor of ~ 100. The best model fit is obtained for the smallest value, and we adopt that here. It might also be possible to assign a value to the diffusivity of dissolved oxygen in bulk water, *D*, but we include this in a lumped transport parameter [35], $\Theta = D\phi^m$. A lumped kinetics parameter $K = kS$ may likewise be defined. The two quantities, *W* and t_{crack}, are assumed to equal the observed value (Figure 2) and the value inferred from the postulate of steady-state denudation ($R = W/t_{crack}$ = 1 cm/ 100 y[23]) respectively.

We may then write relations between Θ and K and other parameters using relations (15), (17), and (18) to yield:

$$K = \frac{2.18}{V_{FeO}\rho M t_{crack}}\left(\frac{1.44x^*}{W}\right)^{\frac{3}{5}}$$
$$\Theta = \left(\frac{W}{1.44}\right)^2\left(\frac{r\rho f_0 M\tau}{c_R}\right)K \quad (19)$$

The observed mean value of W is 2.6 cm (Figure 2). We calculate that t_{crack} is 260 y by assuming that the linear rate of reaction front propagation by fracturing equals the estimated mean rate of denudation for the watershed, ~1 cm/100 yr. These values together then yield the estimates:

$$K = kS \cong 7.8\times10^{-11}\left(\frac{mol_{FeO}}{m^2{}_{FeO}\,s}\right)\left(\frac{m^2{}_{FeO}}{gm_{FeO}}\right)$$
$$\Theta = D\phi^m \cong 5\times10^{-6}\left(\frac{cm^2}{s}\right) \quad (20)$$

Estimates of the separate parameters *k* and *S* (Table 1) reasonably fit the value of *K* (equation 20). A conventional estimate for diffusivity of aqueous solutes in water, $D \approx 10^{-5}$ cm^2/s, requires an unrealistically high value of porosity of $\phi = 0.5$ in the case that $m = 1$. Values for *m*, an empirical exponent used to estimate diffusivity of aqueous solutes in porous media, generally vary between 1 and 3; however, higher values of the exponent *m* would call for an even larger porosity. Few measurements of *m* have been made for low-porosity solids such as the quartz diorite investigated here; however, Brace et al. [36] suggested that values of *m* are often less than 2 for granitic rocks. The defensible choices of $\phi = 0.01$ and $m = 1$ require $D = 5\times10^{-4}$ cm^2/s. Given the uncertainties of estimating diffusivity of species in porous media, this value, within 1.5 orders of magnitude of the conventional value, is acceptable.

The values of Λ and α derived from the model and (18) are:

$$\Lambda = 0.0572$$
$$\alpha = 6.32\times10^{-9} \quad (21)$$

With these values, the model produces an adequate fit of the model to field observations (Fig. 1b).

Model Implications

The weathering advance rate, ω, can be explicitly expressed as W/t_{crack}:

$$\begin{aligned}\omega\left(\frac{cm}{s}\right) &= \frac{W}{t_{CRACK}} \\ &= 0.660\left(\frac{\alpha}{\Lambda^{\frac{4}{5}}}\right)\left(\frac{x^*}{t^*}\right) \\ &\cong 0.660\left(\rho MK\right)^{\frac{1}{5}}\left(\frac{\Theta c_R}{r\tau}\right)^{\frac{4}{5}}\left[\frac{E\left(\frac{1}{3}\frac{\Delta V}{V}\right)^2}{2\Gamma\left(1-\nu\right)}\right]V_{FeO}{}^{\frac{3}{5}}\end{aligned} \tag{22}$$

A notable result is that the dependence on the lumped kinetic parameter, K, is much weaker than the dependence upon the lumped transport parameter Θ. Thus, the controls on weathering rate advance will not follow simple predictions for mineral dissolution: for example, the apparent activation energy of weathering rate advance for this type model would be expected to be significantly smaller than the activation energy for mineral dissolution. Such a discrepancy has been observed by researchers reporting apparent activation energies that are in some cases 2-4 times lower for field observations of weathering as compared to silicate weathering rates in the laboratory [3].

Figure 4b documents that the concentration of oxygen in pore fluid in the rock separating rindlets is never significantly different from c_R except inboard of the youngest fracture. To estimate the extent of reaction within the first-formed rindlet, ξ_1, the second equation in (13) is therefore simplified by setting $c = c_R$, or C = 1. This first-formed rindlet has been reacting with porefluid over the entire time, T. Therefore, by separating variables and integrating from $T = 0$ to T, the following expression for extent of reaction in the outermost rindlet is obtained:

$$\xi_1 = 1 - \exp\left(-\alpha T\right) \tag{23}$$

By inspection, this equation suggests that the reaction of FeO in the outermost rindlet can be thought of as a first-order reaction with rate constant α/t* (compare equation (17)).

We may also approximate the model profiles of reaction extent as a function of space and time, $\xi(x, t)$, by means of the simple relation (23). However, relation (23) was obtained specifically for ξ_1 from an integration over $T = 0$ to T, in recognition that the outermost rindlet reacts over the entire time interval T. In contrast, significant reaction at any point x inboard of that first rindlet occurs only over the time duration during which that point has been situated outboard (nearer the saprolite) of a fracture. In effect, each rindlet only interacts with reservoir porefluid over the time duration dictated by when the rindlet-defining fracture occurs for that point. To determine extent of reaction for each position x, ξ_x, we therefore integrate over this time period, i.e., from $T = 0$ to $T = (t-(t_{crack}/W)x + t_{crack})/t^*$. We obtain:

$$\xi_x = 1 - \exp\left(-kS\left(V_{FeO} M \rho f_0\right)\left[t - \left(\frac{t_{crack}}{W} \right) x + t_{crack} \right] \right), \qquad (24)$$

which only applies when the argument in brackets is greater than zero. Relative to the fixed coordinate origin, $x = 0$, the expression in brackets indicates that the reaction front moves inwards at a velocity $\frac{W}{t_{crack}}$. As each new fracture forms (Fig. 4b), reaction of the "pristine" corestone jumps inward due to influx of reservoir porefluid into the fracture and a quasi-stationary reactant profile is rapidly established. The apparent rate constant is the term external to the bracket (apparent rate constant = $\alpha/t^* = kSV_{FeO}M\rho f_o$); it differs from the chemical rate constant parameter kS by a factor of approximately 10^{-1} (0.072).

Expression (24) predicts that a quasi-stationary reaction front propagates downward into pristine bedrock at a rate of $\frac{W}{t_{crack}}$. As such, this quasi-stationary state is no different than reaction fronts predicted for reactive transport under the condition of pure advection control [33]. Specifically, however, the rate of front advance is determined by the rate of fracturing: it is this rate that controls access of porefluid into the rock that is not in equilibrium with the rock, driving forward reaction.

As rindlets age and continue to react, they will eventually become indistinguishable from saprolite. We define the extent of reaction where this occurs as ξ_{max}. In a steady state weathering system, the number, N, of such rindlets across a set

should be constant in time. We may use equation (23) together with the second relation in (18) to calculate the number of rindlets in a sequence such that the extent of reaction in the oldest rindlet equals the steady state value ξ_{max}:

$$N = \frac{T\left(\xi_{\max}\right)}{T_{crack}} = \frac{-\ln\left[1-\xi_{\max}\right]}{2.18\Lambda^{\frac{3}{10}}} \tag{25}$$

Using this relation, we calculate the extent of reaction of FeO for the number of rindlets observed in a typical rindlet set in Puerto Rico, N=15, 1 - $\xi_{max} = 10^{-6}$. The exponential dependence of reaction extent on fracture number indicates that changes in reaction extent after N = 3 or 4 are not significant. Indeed, we know that the change in FeO reaction extent is not the sole criterion for transition from rindlets to saprolite. Given that fluid infiltration into rindlets accompanies the FeO transformation, and that the volumetrically more important feldspar is also observed to quantitatively react across the rindlet zone, it is inferred that the FeO transformation controls fracturing at the rindlet-corestone interface but that the plagioclase transformation controls the transition from rindlet to saprolite. The rates of these two processes are coupled through the development of porosity and permeability in the rindlets driven by FeO reaction-enhanced fracturing. A smaller value of α for plagioclase (related to the rate constant for plagioclase alteration) is thus predicted, consistent with a higher value of N in equation (25).

The extent of reaction of ferrous mineral within a sequence of rindlets as predicted by the model is comparable to field observations (Fig. 1b), although heterogeneity and temporal variation in conditions in the natural system may cause considerable excursions in the measured mineral concentrations. In Fig. 1b, model output is compared to calculated values of mineral reaction, here expressed as $\tau_{j,w}$. This parameter is defined following accepted models [37] for isovolumetric weathering as:

$$\tau_{j,w} = \frac{c_{j,w}c_{i,p}}{c_{j,p}c_{i,w}} - 1 \tag{26}$$

where $c_{j,k}$ or $c_{i,k}$ are the concentrations of element *j* or *i* respectively in the weathered ($k=w$) or parent ($k= p$) rock. The value of $c_{i,k}$ is calculated assuming one element is immobile (here, Ti is assumed immobile). The parameter $\tau_{j,w}$, which equals 1 for a rock that has altered insignificantly compared to the parent rock composition and 0 for a rock

that has lost all of the mobile component, thus may be compared with the model quantity ξ. Weathering of the Puerto Rico granite has been shown to be isovolumetric [16]: the strain accumulation inherent in our model that causes fracturing is insignificant in calculation of $\tau_{j,w}$.

Although the model predicts extent of reaction of FeO, we do not calculate $\tau_{Fe,w}$ because this value remains essentially constant across the rindlets due to ferric oxide precipitation. In the parent rock, FeO resides predominantly in biotite and hornblende. Petrographic evidence suggests that both these minerals react across the rindlets [38, 39]; however, biotite reaction is incomplete across the rindlets and largely alters to kaolinite + gibbsite in the overlying saprolite while hornblende alteration is quantitative across the rindlets, since no hornblende is observed in the saprolite. Therefore, we assume that the reaction that drives fracturing in the corestone is largely related to hornblende weathering with minor contribution from biotite weathering. To track extent of reaction of hornblende, we track loss of Mg across the rindlets as shown in Figure 1b. $\tau_{Mg,w}$ for hornblende was calculated by assuming that all Mg loss in the rindlet zone is from hornblende weathering and by using a parent rock Mg composition that reflects only the Mg in the hornblende based on petrographic data of Turner et al. [38].

As explained earlier, in applying the model we have assumed invariant c_R: if we relax this assumption and allow time-varying reservoir conditions, the extent of reaction in successive rindlets still varies monotonically (Figure 5). Therefore, noise in the observed chemical data shown in Fig. 1b cannot be explained by variations in c_R, but must rather be related to spatial variations in rock porosity or composition.

Weathering and denudation

As noted earlier, if we calculate weathering advance rate for the no-fracture case (Fig. 4a), the reaction front moves inward at a rate $\propto t^{1/2}$: this model demonstrates so-called parabolic kinetics expected for formation of a surface alteration layer that is rate-limited by diffusion across the layer[40]. Such parabolic kinetic behavior is not consistent with steady state weathering rate advance because rates are not time-invariant. Surprisingly, as shown here, such constancy in time characterizes a spheroidal weathering model wherein advance rate is controlled by coupling between transport,

reaction, and mechanical properties. The spheroidal weathering model with fracturing shows that crack spacing and time intervals between cracking events are uniform, consistent with steady-state weathering (Fig. 4b). As pointed out earlier, for the spheroidally fracturing system and for a given c_R, once the reacting mineral is depleted from volume fraction f_o to 0 in the outer alteration zone, a quasi-stationary state is established [33] wherein the entire reaction front remains unchanging in shape but moves inward into the corestone at a steady-state rate $\omega = W/t_{crack}$. Importantly, while weathering advance rates that are constant in time have generally been interpreted in the literature as rate limitation not by transport but by the mineral-water interface reaction, results presented here can explain why transport-limited weathering can still yield weathering advance rates that are linear with respect to time[41].

The model presented for the no-fracture case shows parabolic kinetics ($\propto t^{1/2}$) largely because of the assumption of an immobile boundary condition. However, if we suppose that the external boundary at X = 0, where $c = c_R$, migrates downward with time in steady state with the rate of denudation, R, then we can implement a third, fully steady-state model. The front at X = 0 must necessarily be supposed to be the front at which saprolitization is complete, even though we do not treat this reaction in these models. The large porosity in this material then allows the reservoir concentration to be maintained at the front. The result (Figure 6) is a narrow zone of formation of ferric oxide for $C \geq C_N$. When R = 0.01 cm/a, the observed rate for the Rio Blanco system, little precipitation of $Fe(OH)_3$ occurs in this zone, and further reaction of FeO must then continue in the saprolite. Reduction of the rate of erosion by a factor of 1/10 still leads to a narrow zone, only ~ 1.5 times thicker than that of the previous case, but the extent of reaction, ξ, is much larger. These calculations show that for both the no-fracture and with-fracture cases, weathering advance rates can be constant in time. However, the calculations emphasize that the rate of saprolitization inferred for the no-fracture system could only be in steady-state with a rate of denudation far smaller than that observed for the Rio Blanco quartz diorite. Without fracturing, the saprolite cover would be removed faster than the weathering advance rate, exposing essentially bare bedrock, and a qualitatively different scheme of weathering and erosion would be required.

In a weathering profile where soil + saprolite thickness is at steady state, the weathering advance rate, ω, equal to the rate of saprolite formation from bedrock, must equal both the rate of soil formation from saprolite and the rate of loss of soil to chemical + physical erosion, *R*. For the spheroidal weathering model, the rate of denudation must equal ω at steady state, and this balance then determines the steady-state value of c_R:

$$c_R^{0.25} = \left(\frac{R}{q} \right)^{5/4} \tag{27}$$

where *q* is a constant dependent upon rock and mineral composition that describes transport, reaction kinetics, and mineral volumetric and fracture properties. For such a system, if *R* increases, the saprolite thickness will decrease and c_R will increase toward c_{atm}, the dissolved O_2 concentration in equilibrium with the atmosphere (Table 1). As c_R increases, the rate of propagation of the weathering front will increase until ω equals *R*. Thus a positive feedback controls the thickness of the regolith. The spheroidal weathering model provides a mechanism to explain how bedrock disaggregation can be caused by chemical weathering; hence, the model allows equal rates of chemical weathering and denudation [3] to be reconciled.

In applying the spheroidal weathering model to the Rio Icacos quartz diorite, we used a value of c_R as published by White et al. [16] for pore fluid sampled by lysometer at 8.5 m depth. In sampling this water, no attempts were made to keep atmospheric oxygen from interacting with the sample (White, A., pers. comm.). The value of c_R, a major unknown in the model, could vary significantly toward very low values depending upon the connectivity between the reservoir and the overlying atmosphere. Reservoir oxygen concentrations will generally decrease downward as oxygen is used up through oxidation of reduced minerals within regolith. Furthermore, biotic reactions will typically use oxygen and create more reducing conditions at the bottom of weathering regolith as compared to surficial systems. For simplicity, we here assume that c_R varies with the depth of soil + saprolite, *z*, according to a simple relationship incorporating a linear depth coefficient, *b*:

$$c_R = c_{atm} + bz \tag{28}$$

We can solve (27) and (28) to determine how the steady state thickness of the soil, z_{ss}, is dependent upon atmospheric O_2, total denudation rate, and other chemical and physical parameters captured in q:

$$z_{ss} = \frac{1}{b}\left(\left(\frac{R}{q}\right)^5 - c_{atm}\right) \tag{29}$$

Because b is negative ($c_R < c_{atm}$), $(R/q)^5$ must be less than c_{atm} under steady state conditions to achieve a nonzero soil thickness.

This formulation emphasizes that, as erosion rate increases at constant atmospheric O_2, the soil thickness at steady state decreases. Such a result is expected from the model because as R increases and z_{ss} decreases, c_R increases, causing a higher rate of weathering (e.g. W increases and t_{crack} decreases). Similarly, over geologic time, as O_2 increases (e.g.[42]), the bedrock to saprolite conversion rate must increase, creating thicker soil profiles for a given denudation rate. To illustrate these effects, a change in R was simulated using our model by allowing weathering to occur for an amount of time and then assuming that erosion decreased (soil thickness increased) to the extent that c_R halved. Figure 5 shows that when c_R halves, W and t_{crack} both increase, documenting a decrease in weathering advance rate, W/t_{crack}.

For observations of rindlets in natural systems, it therefore may be assumed that the weathering system has operated at steady state if the spacing between fractures remains constant. In the Rio Blanco granite, spacing averages 2.6 cm, consistent with steady state weathering rate advance. The slightly larger rind thicknesses observed for the youngest rinds may be consistent with splitting of rindlets with age (Figure 1,2).

Erosion in the Rio Icacos watershed is known to be characterized by frequent landslides. In a 275 km^2 study area including the Rio Icacos watershed, landslide frequency was found to average 0.8 landslides km^{-2} $decade^{-1}$ on forested hillslopes [43]: i.e. a rate of 10^{-7} landslides m^{-2} y^{-1}. Given that spheroidal weathering rinds are commonly observed throughout this watershed, if steady state weathering has occurred and if large landslides are assumed to scrape off saprolite + most of the rindlet set at any given time, we must conclude that the amount of time needed to develop the steady state rindlet set (N = 15, or 3900 yr) must be less than the average landslide recurrence interval.

Estimating from outcrop observation that consistent spheroidally weathered rindlet sets are characteristic of an area of 100 m^2 in any given location, then over this land area the recurrence interval between landslides is approximately 10^5 y. Clearly, our estimated time duration of rindlet set formation, 3900 y, is well within the landslide recurrence interval for such an area, suggesting that steady state conditions can be obtained. Erosive loss of material from the top of the saprolite/soil column between large landslides, occurring by small landslide or other forms of transport, controls the steady state thickness described in equation (29). Observations of rindlet thickness and rindlet set thickness, as well as reaction extent variation across rindlet sets, for this and other spheroidally weathering regimes may yield evidence of landslide frequency or time variance of erosion rate.

Conclusions

Surprisingly, despite the first-order nature of the process, no quantitative models are available to answer the question: how does bedrock disaggregate to form soil? However, many if not all, models for landscape evolution implicitly or explicitly rely upon assumptions of time-invariant soil and saprolite thickness. Such assumptions implicitly assume that rates of chemical weathering and rates of bedrock transformation into bedrock are constant in time.

Spheroidal weathering is a common mechanism by which intact bedrock transforms to saprolite. The phenomenon is found on almost all continents and rock types and in many climate regimes. We present a model for spheroidal weathering that explicitly couples the physical process of fracturing that leads to disaggregation and formation of saprolite to the chemical processes during water-rock interaction. Surprisingly, the model documents that reaction-enhanced fracturing is limited by both chemical reaction kinetics and transport and yet yields a weathering advance rate that is linear in time, as needed to explain time-invariant thickness of soils and saprolite. Linearity with respect to time is demanded by our model because the time between fracturing is constant -- dictated by the time needed to achieve the reaction extent required for accumulated strain energy to equal fracture surface energy -- and the fracture frequency dictates the rate of advance of the weathering front.

Linear weathering advance rates are also predicted for a model where weathering of the rock is rate-limited by diffusive mass transfer without fracturing, as long as erosion removes soil/saprolitic material from the top of the column. However, in this no-fracture, moving-boundary value model, the weathering rate advance must be slower than in the fracturing case: in effect, the faster rate of weathering rate advance in the spheroidal fracture model is controlled by the time duration over which the rock interacts with non-equilibrated porefluid, which increases markedly with fracturing. The rindlet-defining fractures accelerate the access of corrosive fluid into pristine bedrock.

The apparent rate constant for mineral alteration that is implied by the spheroidal weathering model is significantly slower than mineral alteration rates measured in the laboratory (because rates of transport control the weathering advance rate more than chemical rates of alteration). This inference is consistent with the observation that most estimates of apparent rate constants for mineral weathering derived from soils developed on bedrock are orders of magnitude slower than estimates for such weathering rates in the laboratory.

The model documents that the rate of weathering interface advance depends on the concentration of reactant in pore fluid at the saprolite-bedrock interface: this value couples the physical and chemical processes of soil removal and chemical weathering respectively. For the Puerto Rico quartz diorite investigated here, we postulate that the critical reactant is dissolved oxygen in pore fluid. As in many other weathering profiles, one of the earliest reactions in the pristine bedrock is oxidation of ferrous minerals. Precipitation of ferric minerals is shown to cause strain and subsequent fracturing of the rock. Extrapolating from our observations in Puerto Rico, the dissolved oxygen in soil and saprolite porewaters may therefore be an important control on rates of bedrock disaggregation and the rate of drawdown of carbon in the atmosphere due to silicate weathering. The need for such coupling between the oxygen and carbon cycles has been postulated in the literature but our model is the first observationally based model to propose an explicit coupling.

Further investigations of spheroidal weathering will provide more insight into the coupling of physical and chemical processes and coupling between the carbon and oxygen cycles.

Acknowledgements

We thank J. Troester, A. White, D. Mericle, and G. Hernandez for field support and P. Sak for analytical assistance. We thank two reviewers for their incisive comments. Funding provided by DOE grant DE-FG02-05ER15675, NSF-IGERT grant DGE-9972759, the Penn State Center for Environmental Chemistry and Geochemistry, and ACS-PRF grant 40877-AC8. H. Buss acknowledges fellowship support of the NSF Graduate Research Fellowship Program.

Table 1. Physicochemical parameters describing Rio Blanco granite

Parameters	Symbol	Value
Estimated from literature		
Fracture surface energy	Γ	2×10^5 dyne/cm^2
Poisson's ratio	ν	0.25
Young's modulus	E	10^{12} dynes/cm^2
Specific surface area of reacting mineral[a]	S	0.2 m^2 gm^{-1}
Density of reacting mineral[b]	ρ	3 gm/cm^3
Specific volume of FeO	V_{FeO}	12 cm^3 mol^{-1}
Tortuosity of corestone	τ	3
Rate constant for FeO dissolution[c]	k	3.9×10^{-10} mol/m^{2}s
Concentration of dissolved O_2 in pore fluid at bedrock-saprolite interface[d]	c_R	2.3×10^{-7} mol/cm^3
Concentration of dissolved O_2 in equilibrium with bedrock	c_{eq}	0 mol/cm^3
Concentration of dissolved O_2 in equilibrium with atmosphere	c_{atm}	2.6×10^{-7} mol/cm^3
Time interval between cracking	t_{crack}	260 y
Weathering advance rate	ω	~0.01 cm y^{-1}
Assumed for model (see text)		
Stoichiometric coefficient	r	¼
Diffusion coefficient	D	5×10^{-4} cm^2/s
Porosity of corestone	ϕ	0.01
Porosity exponent	m	1
Lumped kinetics parameter	$K(=kS)$	7.8×10^{-11} mol gm^{-1} s^{-1}
Relative volume change[e]	$\Delta V/V$	0.05
Volume fraction FeO (all Fe as FeO)[f]	f_0	0.05
Concentration of dissolved O_2 when nucleation rate of ferrihydrite = 0	c_N	0.1 c_R
Estimated from observation		
Mole fraction of FeO in rock	M	0.04
Mean fracture spacing	W	2.6 cm

[a]The specific surface area of hornblende [44] for the grain size observed in rock (= 150 - 250 μm).
[b]Density of hornblende [32].
[c]Rate constant for dissolution of FeO as a function of pH ($k(pH)$) was estimated from dissolution rate constants at pH 2 for metal oxides assuming that n ($\log k(pH) = \log k_o + n$ pH) equals -0.7 and $k_o = 1.4 \times 10^{-5}$ mol m^{-2} s^{-1} as per [45]. Porefluid pH was assumed = 7 (more alkaline than the pH 5.1 measured at bedrock-saprolite interface [16] due to the low water-rock ratio).
[d]Calculated from measured $P_{O2} = 0.183$[16] at the corestone-saprolite interface using the Henry's law constant, K_h for oxygen at 25°C = $10^{-2.9}$ M atm^{-1} [46].
[e]This ratio equals 0.7 for equation (2) for wustite to ferrihydrite [32]. However, because we are modeling the FeO component in hornblende, this value is multiplied by the mol fraction of Fe in Rio Blanco hornblende (0.14) x the fraction, Fe(II) / total Fe in the hornblende (assumed = 0.5).
[f]Estimated as f_o = wt. % FeO x ρ_{rock}/ρ_{FeO}, where up to ~10 wt.% FeO has been estimated for Rio Blanco granite [37], ρ_{rock} = 2.7 gm cm^{-3}, and ρ_{FeO} = 5.9 gm cm^{-3}.

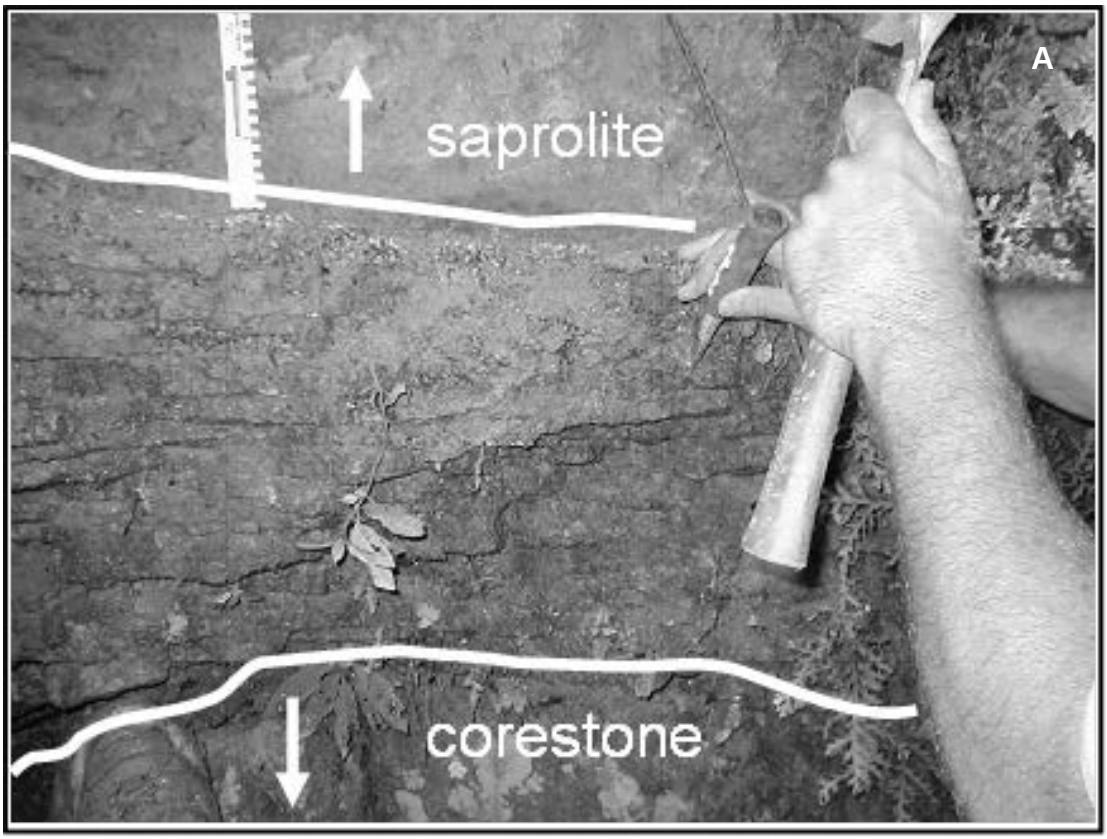

Figure 1a.

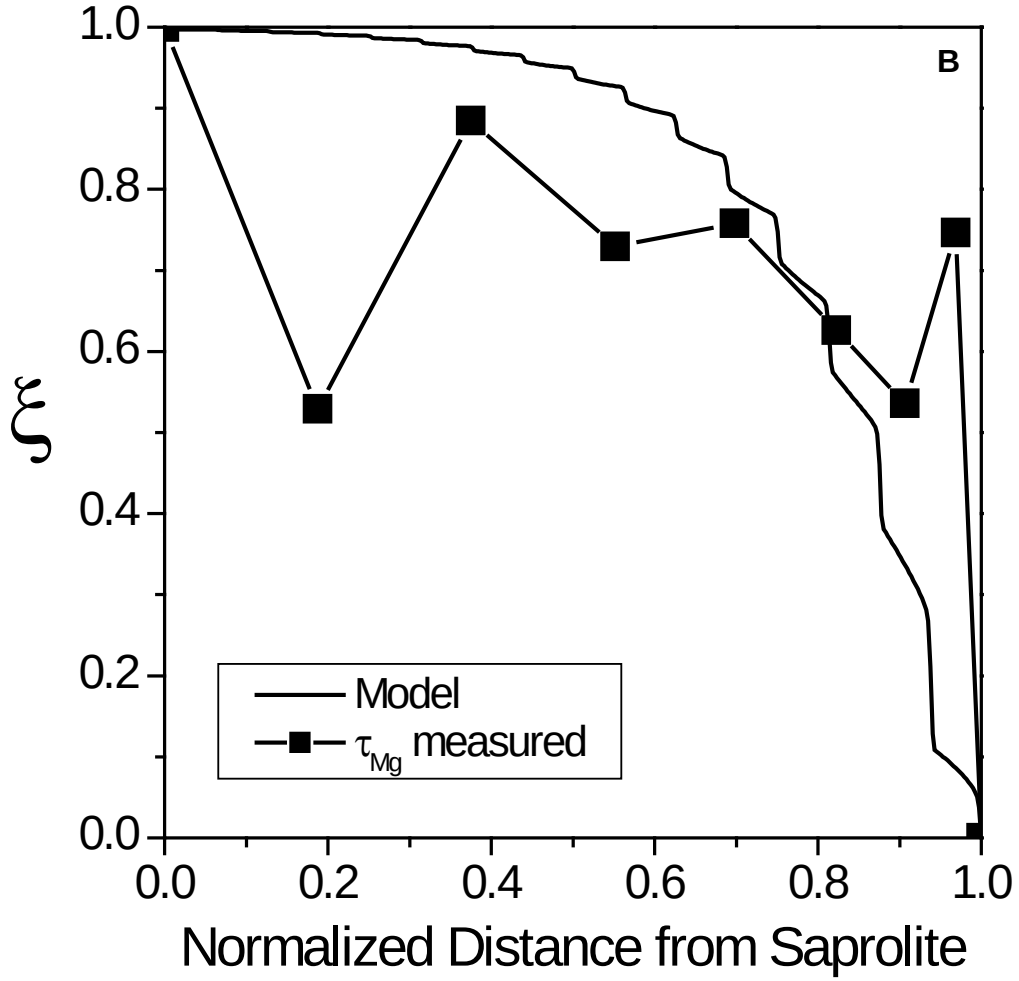
B
1.0
0.8
0.6
0.4
0.2
0.0
ξ
Model
τMg measured
0.0
0.2
0.4
0.6
0.8
1.0
Normalized Distance from Saprolite

Figure 1b

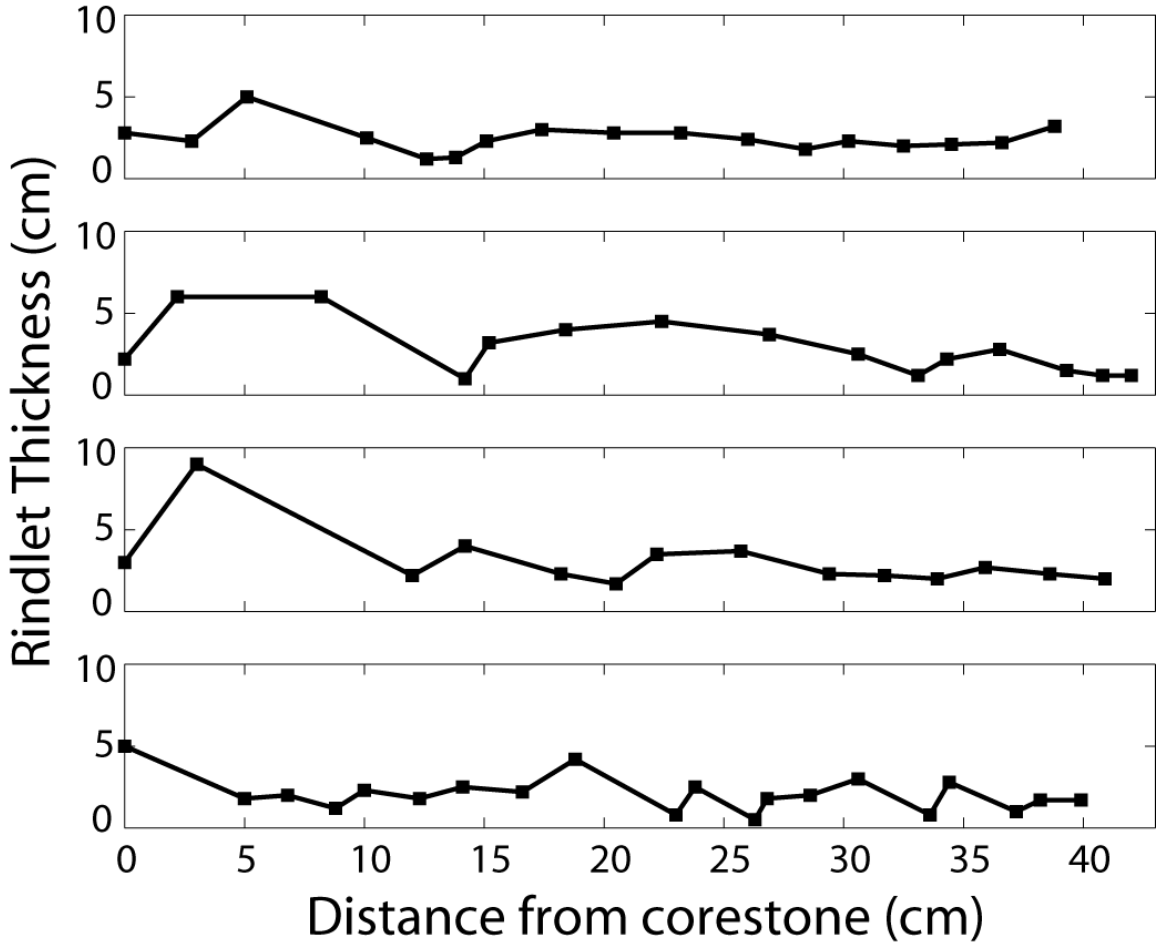
Rindlet Thickness (cm)
10
5
0
10
5
0
10
5
0
10
5
0
0
5
10
15
20
25
30
35
40
Distance from corestone (cm)

Figure 2.

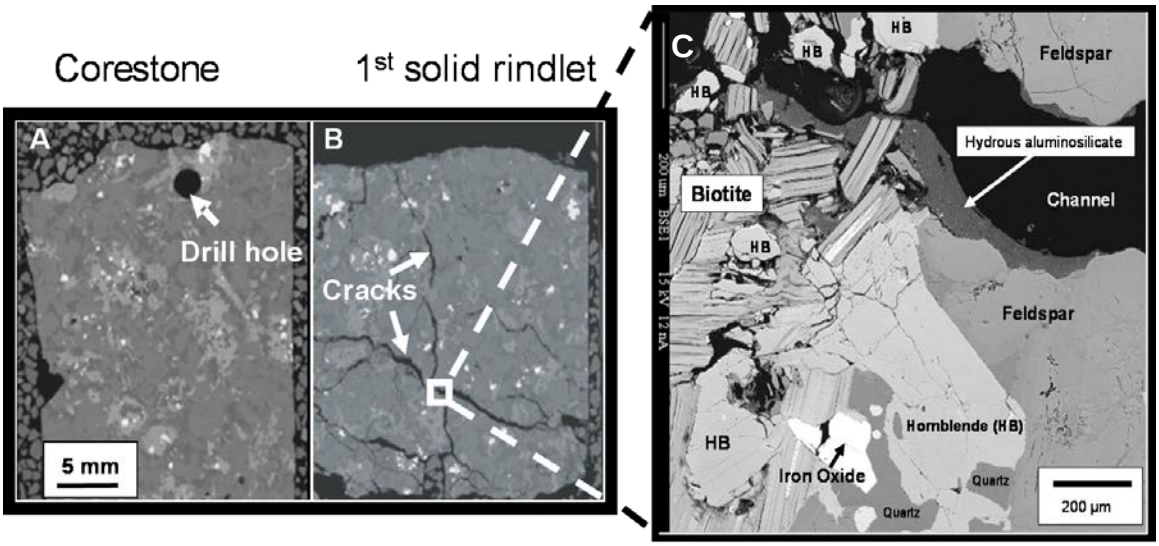
Corestone
1st solid rindlet
A
B
C
Drill hole
Cracks
5 mm
HB
Feldspar
Hydrous aluminosilicate
Channel
Biotite
Feldspar
Hornblende (HB)
Iron Oxide
Quartz
Quartz
200 µm

Figure 3.

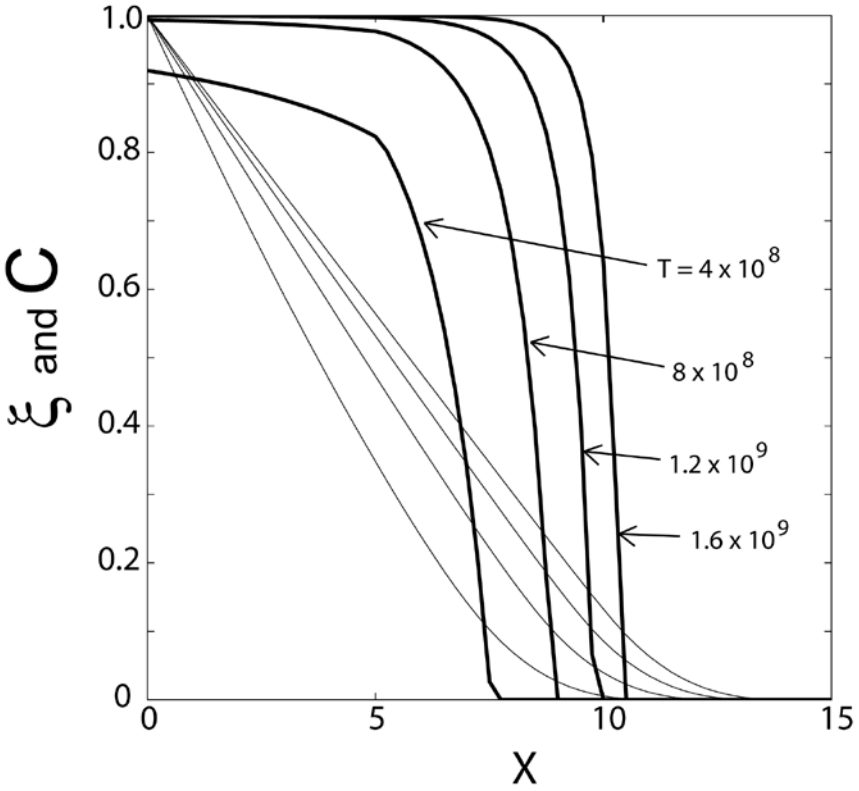

Figure 4a

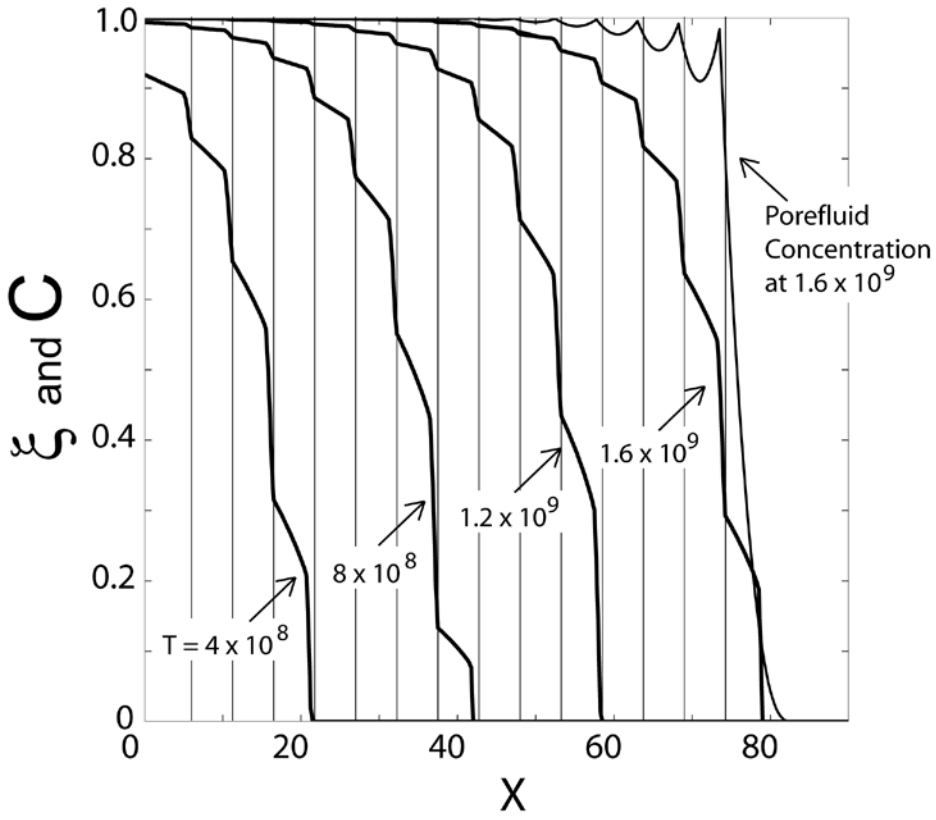
1.0
0.8
0.6
0.4
0.2
0
0
20
40
60
80
X
ξ and C
Porefluid
Concentration
at 1.6 x 10^9
1.6 x 10^9
1.2 x 10^9
8 x 10^8
T = 4 x 10^8

Figure 4b

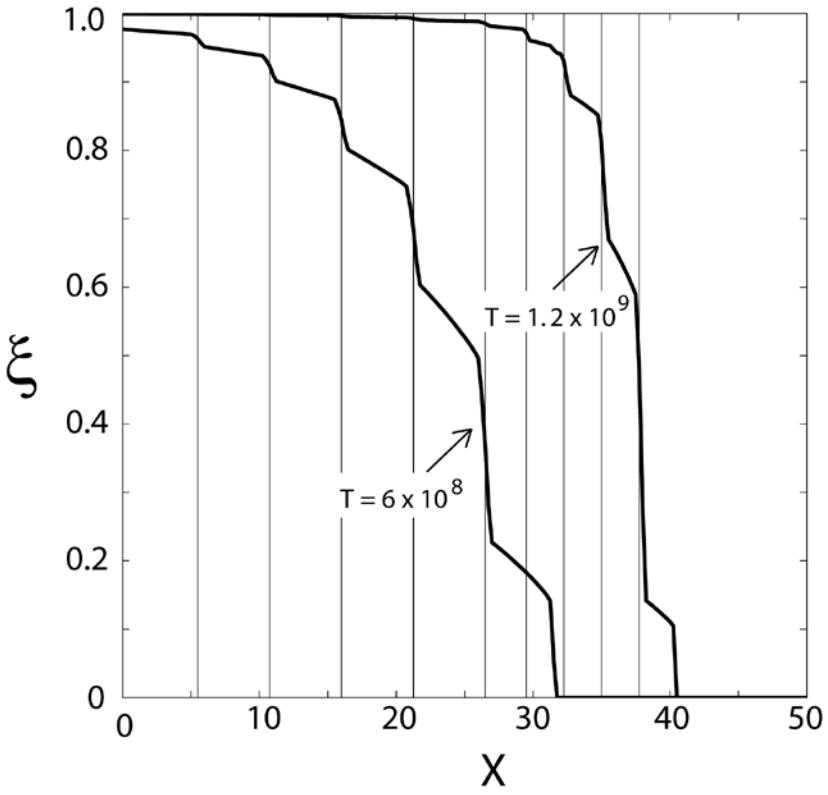

Figure 5.

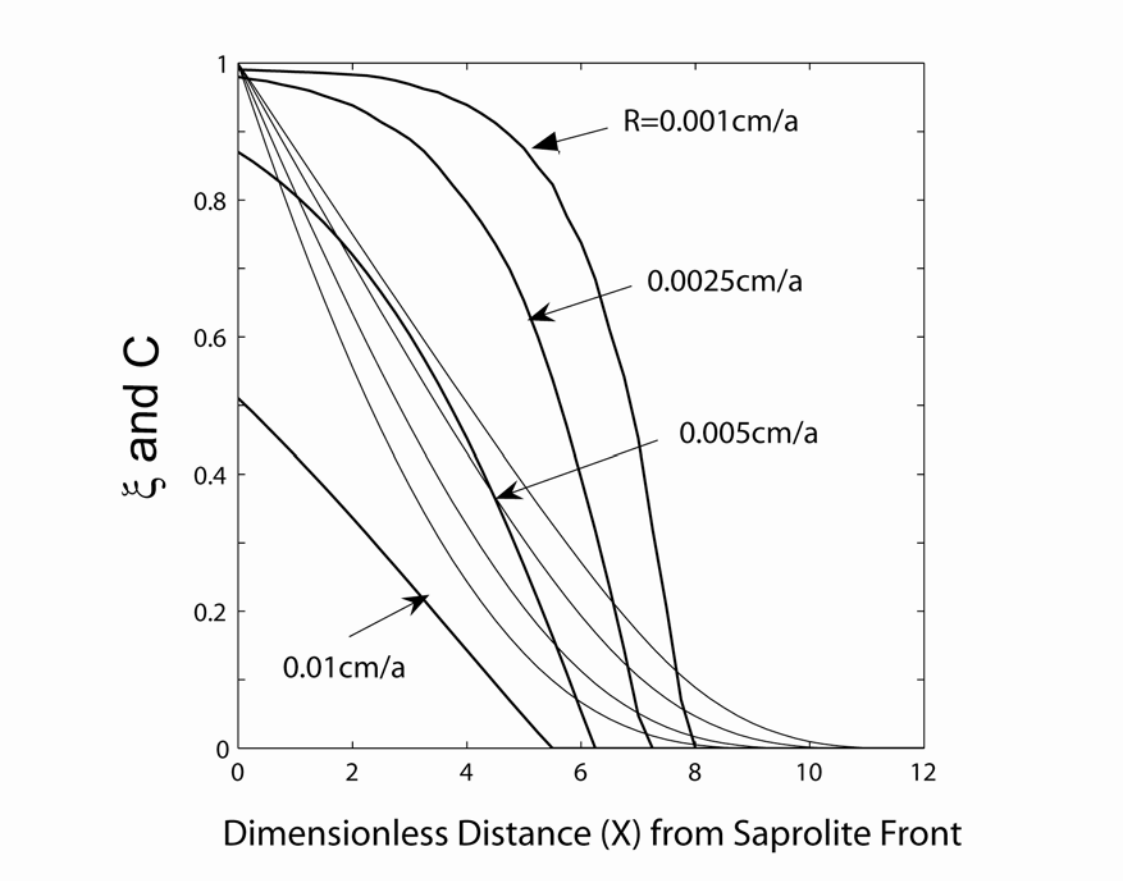
R=0.001cm/a
0.0025cm/a
0.005cm/a
0.01cm/a
ξ and C
Dimensionless Distance (X) from Saprolite Front
0
0.2
0.4
0.6
0.8
1
0
2
4
6
8
10
12

Figure 6.

References

[1] F. van Blackenburg, T. Hewawasam, P.W. Kubik, Cosmogenic nuclide evidence for low weathering and denudation in the wet, tropical highlands of Sri Lanka, Geophysical Research-Earth Surface 109(2004).

[2] A.M. Heimsath, W.E. Dietrich, K. Nishiizumi, R.C. Finkel, The soil production function and landscape equilibrium, Nature 388(1997) 358-361.

[3] C.S. Riebe, J.W. Kirchner, R.C. Finkel, Erosional and climatic effects on long-term chemical weathering rates in granitic landscapes spanning diverse climate regimes, Earth and Planetary Science Letters 224(2004) 547-562.

[4] C.D. Ollier, Causes of spheroidal weathering, Earth-Science Reviews 7(1971) 127-141.

[5] C.D. Ollier, Spheroidal weathering, exfoliation and constant volume alteration, Zeitschrift fuer Geomorphologie 11(1967) 103-108.

[6] A. Chatterjee, B.C. Raymahashay, Spheroidal weathering of Deccan Basalt: a three-mineral model, Quarterly Journal of Engineering Geology 31(1998) 175-179.

[7] S.J. Fritz, D.W. Mohr, Chemical alteration in the micro weathering environment within a spheroidally-weathered anorthosite boulder, Geochimica Cosmochemica Acta 48(1984) 2527-2535.

[8] M.T. Heald, T.J. Hollingsworth, R.M. Smith, Alteration of sandstone as revealed by spheroidal weathering, Journal of Sedimentary Petrology 49(1979) 901-909.

[9] R.W. Chapman, M.A. Greenfield, Spheroidal weathering of igneous rocks, American Journal of Science 247(1949) 407 - 429.

[10] E. Le Pera, M. Sorriso-Valvo, Weathering and morphogenesis in a mediterranean climate, Calabria, Italy, Geomorphology 43(2000) 251-270.

[11] J.M. Ferry, Landforms of spheroidally weathered rock, in: T.L. Smiley, J.D. Nations, T.L. Pewe, J.P. Schafer, (Eds), Landscapes of Arizona, University Press of America, Lanham, MD, 1984, pp. 415-427.

[12] D. Isherwood, A. Street, Biotite-induced grussification of the Boulder Creek Granodiorite, Boulder County, Colorado, Geological Society of America Bulletin 87(1976) 366-370.

[13] M.A. Sequeira Braga, H. Paquet, A. Begonha, Weathering of granites in a temperate climated (NW Portugal): granitic saprolites and arenization., Catena 49(2002) 41-56.

[14] C.D. Ollier, Deep weathering, groundwater and climate, Geografiska Annaler., Series A, Phys. Geog. 70(1988) 285-290.

[15] P. Mignon, M.F. Thomas, Grus weathering mantles - problems of interpretation, Catena 49(2002) 5-24.

[16] A.F. White, A.E. Blum, M.S. Schulz, D.V. Vivit, D.A. Stonestrom, M. Larsen, S.F. Murphy, D. Eberl, Chemical weathering in a tropical watershed, Luquillo Mountains, Puerto Rico: I. Long-term versus short-term weathering fluxes, Geochimica et Cosmochimica Acta 62(1998) 209-226.

[17] M.S. Schulz, A.F. White, Chemical weathering in a tropical watershed, Luquillo Mountains, Puerto Rico: III. Quartz dissolution rates, Geochimica et Cosmochimica Acta 63(1999) 337-350.

[18] S.F. Murphy, S.L. Brantley, A.E. Blum, A.F. White, H. Dong, Chemical weathering in a tropical watershed, Luquillo Mountains, Puerto Rico; II. Rate and mechanism of biotite weathering, Geochimica et Cosmochimica Acta 62(1998) 227-243.
[19] A.F. White, T.D. Bullen, M.S. Schulz, A.E. Blum, T.G. Huntington, N.E. Peters, Differential rates of feldspar weathering in granitic regoliths, Geochim. Cosmochim. Acta 65(2001) 847-869.
[20] A.F. White, Determining mineral weathering rates based on solid and soute weathering gradients and velocities: application to biotite weathering in saprolites, Chemical Geology 190(2002) 69-89.
[21] C.S. Riebe, J.W. Kirchner, R.C. Finkel, Long-term rates of chemical weathering and physical erosion from cosmogenic nuclides and geochemical mass balance, Geochimica et Cosmochimica Acta 67(2003) 4411-4427.
[22] B.F. Turner, R.F. Stallard, S.L. Brantley, Investigation of in situ weathering of quartz diorite bedrock in the Rio Icacos basin, Luquillo Experimental Forest, Puerto Rico, Chemical Geology 202(2003) 313-341.
[23] E.T. Brown, R. Stallard, M.C. Larsen, G.M. Raisbeck, F. Yiou, Denudation rates determined from the accumulation of in situ-produced ^{10}Be in the Luquillo Experimental Forest, Puerto Rico, Earth and Planetary Science Letters 129(1995) 193-202.
[24] E.S. Larsen, Batholith and associated rocks of Corona, Elsinore and San Luis Rey quadrangles, southern California, Geological Society of America Memoir 29(1948) 114-119.
[25] D.R. Simpson, Exfoliation of the Upper Pocohontas sandstone, Mercer County, West Virginia, American Journal of Science 242(1964) 545-551.
[26] T.J. Rice, Jr., S.W. Buol, S.B. Weed, Soil saprolite profiles, derived from mafic rocks in the North Carolina Piedmont. I. Chemical, morphological, and mineralogical characteristics and transformations, Soil Sci. Soc. Am. J. 49(1985) 171-178.
[27] I. Stephen, A study of rock weathering with reference to the soils of the Malvern Hills. II. Weathering of appanite and ivy scar rock, J. Soil. Sci. 3(1952) 20-33.
[28] A.L. Boettcher, Vermiculite, hydrobiotite, and biotite in the Rainy Creek igneous complex near Libby, Montana, Clay Minerals 6(1966).
[29] D.H. Eggler, E.E. Larson, W.C. Bradley, Granites, grusses, and the Sherman erosion surface, southern Laramie Range, Colorado-Wyoming, American Journal of Science 267(1969) 510-522.
[30] D.S. Fanning, V.Z. Keramidas, M.A. El-Desoky, Micas, in: S.B. Weed, (Ed), Minerals in Soil Environments, Soil Science Society of America, Madison, Wisconsin, 1989, pp. 551-624.
[31] T. Murakami, S. Utsunomiya, T. Yokoyama, T. Kasama, Biotite dissolution processes and mechanisms in the laboratory and in nature: Early stage weathering environments and vermiculization, American Mineralogist 88(2003) 377-386.
[32] R.A. Robie, B.S. Hemingway, Thermodynamic properties of minerals and related substances at 298.15 K and 1 bar (10 (super 5) Pascals) pressure and at higher temperatures, U. S. Geological Survey Bulletin, Report, 1995, p. 461.

[33] P.C. Lichtner, The quasi-stationary state approximation to coupled mass transport and fluid-rock interaction in a porous medium., Geochimica et Cosmochimica Acta 52(1988) 143-165.
[34] M. Friedman, J. Handin, G. Alani, Fracture-surface energy of rocks, International Journal of Rock Mechanics and Mining Sciences 9(1972) 757-766.
[35] E.H. Oelkers, Physical and chemical properties of rocks and fluids for chemical mass transport calculations, in: P.C. Lichtner, C.I. Steefel, E.H. Oelkers, (Eds), Reactive Transport in Porous Media 36, Mineralogical Society of America, 1996, pp. 131-191.
[36] W.F. Brace, A.S. Orange, T.R. Madden, The effect of pressure on the electrical resistivity of water saturated rocks, Journal of Geophysical Research 70(1965).
[37] S.P. Anderson, W.E. Dietrich, G.H. Brimhall, Weathering profiles, mass-balance analysis, and rates of solute loss: Linkages between weathering and erosion in a small, steep catchment, Geological Society of America Bulletin 114(2002) 1143-1158.
[38] B.F. Turner, R.F. Stallard, S.L. Brantley, Investigation of in situ weathering of quartz diorite bedrock in the Rio Icacos basin, Luquillo Experimental Forest, Puerto Rico, Chemical Geology 202, 2003, pp. 313-341.
[39] H.L. Buss, P.B. Sak, A.F. White, S.L. Brantley, Mineral dissolution at the granite-saprolite interface, in: R.B. Wanty, R.R.I. Seal, (Eds), 11th International Symposium on Water-Rock Interaction 11, Taylor and Francis, Saratoga Springs, NY, 2004, pp. 819-823.
[40] R.W. Luce, R.W. Bartlett, G.A. Parks, Dissolution kinetics of magnesium silicates, Geochimica et Cosmochimica Acta 36(1972) 35-50.
[41] P.B. Sak, D.M. Fisher, T.W. Gardner, K.M. Murphy, S.L. Brantley, Rates of weathering and rind formation on Costa Rican basalt, Geochimica Cosmochimica Acta 68(2003) 1453-1472.
[42] T.M. Lenton, The role of land plants, phosphorus weathering and fire in the rise and regulation of atmospheric oxygen, Global Change Biology 7(2001) 613-629.
[43] M.C. Larsen, A.J. Torres-Sanchez, The frequency and distribution of recent landslides in three montane tropical regions of Puerto Rico, Geomorphology 24(1998) 309-331.
[44] S.L. Brantley, N. Mellott, Specific surface area and porosity of primary silicate minerals, American Mineralogist 85(2000) 1767-1783.
[45] W.H. Casey, J.F. Banfield, H.R. Westrich, L. McLaughlin, What do dissolution experiments tell us about natural weathering?, Chemical Geology 105(1993) 1-15.
[46] F.M.M. Morel, J.G. Hering, Principles and Applications of Aquatic Chemistry, John Wiley & Sons, Inc., New York, 1993, 588 pp.

Figure Captions

Figure 1. (a) Rindlet sequence developed between corestone and saprolite at the Route 191 outcrop, El Yunque National Forest, Puerto Rico. In this image, no fractures are imaged in the saprolite nor in the corestone; fractures are only observed in the rindlet zone as indicated. (b) $\tau_{Mg,w}$ profile (solid squares) measured across the rindlet zone transition as compared with a model profile of calculated reacted fraction (ξ plotted as the line, see text). Values of $\tau_{Mg,w}$ were calculated from the observation that all the hornblende was dissolved in the quartz diorite across the rindlet set. For consistency with respect to this comparison to ξ, we have plotted the negative of calculated $\tau_{Mg,w}$ using equation (26): the value of $\tau_{Mg,w}$ thus varies from 1 (at rindlet-saprolite interface where no hornblende remains) to 0 (at corestone-rindlet interface where hornblende concentration is identical to parent).

Figure 2. Four profiles of rindlet thickness versus distance outward from corestone, all measured at the Route 191 outcrop, El Yunque National Forest, Puerto Rico. The mean and median of 123 measured rindlets were 2.6 $\pm$ 1.6 cm and 2 cm respectively.

Figure 3. Backscattered electron maps (BSEM) of thin-sections of Rio Blanco quartz diorite. The top edge of the thin-section in (a) is the edge of a corestone adjacent to the rindlet zone. No secondary porosity is evident in the corestone (sample drill hole is evident). The thin-section in (b) entirely spans the first cohesive weathered rindlet layer above the corestone and is cross-cut by micro-cracks. (c) A BSEM image of a micro-crack formed in the rindlet shown in (b). A hydrous aluminosilicate phase is only observed lining channels. Iron oxides have formed near hornblende and biotite crystals.

Figure 4. (a) Extent of reaction (ξ, dark lines) and profiles of normalized porefluid concentrations of oxygen (C, light lines) for $\Lambda = 0.0572$, $\alpha = 6.32 \times 10^{-9}$, and $c_N = 0.1c_R$ at times $T = 4 \times 10^8$, 8×10^8, 12×10^8, and 16×10^8 , as noted, calculated for (a) the no-fracture and (b) the with-fracture model. In (b) only the last concentration profile is shown, while all C profiles are delineated in (a). Notice that for the with-fracture case, porefluid concentration of oxygen only differs significantly from c_R (C = 1 for porefluid

oxygen concentration = c_R) inboard of the youngest fracture: porefluid concentrations are roughly constant across the reacting zone throughout the rindlet set. In both figures, dimensionless distance from the bedrock-saprolite interface is used as the abscissa (X, X = 0 implies the rindlet-saprolite interface). Note that the rate of advance of the reaction front is nonlinear in time in (a) but linear in time in (b). In (b), the position of fractures once they have formed in the model at 8×10^8 is noted by the dashed lines.

Figure 5. Extent of reaction (ξ) calculated at times $T = 6 \times 10^8$ and 12×10^8, as noted (see Figure 4). The model was run until $T = 6 \times 10^8$ with a constant value of c_R for the parameters $\Lambda = 0.0572$, $\alpha = 6.32 \times 10^{-9}$, and $c_N = 0.1c_R$. At this value of T, c_R was then reduced to half its initial value, and the model was run until $T = 12 \times 10^8$. Since $\Lambda \sim 1/c_R$, this quantity was doubled at $T = 6 \times 10^8$. The value of c_N is fixed relative to c_R so at $T = 6 \times 10^8$, c_N was also adjusted. Note that a reduction in the reservoir porefluid concentration of oxygen results in a decrease in fracture spacing (shown by vertical lines) and decrease in weathering advance rate.

Figure 6. Steady-state weathering profiles of ξ and C within rock for best-fit model parameters, without fracturing, at four different rates of erosion. The X-axis is taken as zero at the moving saprolite/rock boundary, above which the much larger porosity allows rapid transport of porewater oxygen. In these models, FeO continues to react in the saprolite zone, but the profiles of ξ are not continued into this zone.